Composites Communications 26 (2021) 100789

Contents lists available at ScienceDirect

Composites Communications

journal homepage: www.elsevier.com/locate/coco

Hierarchical porous carbon nanofibers with lithiophilic metal oxide crystalline grains for long-life Li metal anodes

Chengcheng Zhao, Xiao Yao, Hao Yang, Xiaoxia Jiao, Lina Wang *

State Key Laboratory for Modification of Chemical Fibers and Polymer Materials, College of Materials Science and Engineering, Donghua University, Shanghai, 201620, China

ARTICLE INFO

Keywords:
Lithium metal anode
Carbon nanofibers
Zinc oxide
Lithiophilic sites

ABSTRACT

The application of rechargeable lithium (Li) metal batteries holds great promise for the next-generation energy storage field. However, the development of metallic Li anode is hindered by the dendrite growth on the surface and volume expansion during cycling. Herein, a composite of ZnO/carbon nanofibers (ZnO/CNFs) is rationally designed as a lithiophilic host for the uniform Li plating/stripping. The introduction of well-dispersed ZnO crystalline grains effectively transfers the lithiophibic carbon nanofibers (CNFs) into lithiophilic. The in-situ created nanoporous structure is able to alleviate the internal stress during repeating Li plating/stripping. The interconnected 3D structure provides abundant electrolyte/Li interfaces, which is beneficial minimizing local current density. Therefore, the ZnO/CNFs@Li composite anode displays a long lifespan of 1900 h along with a low voltage hysteresis of 21.7 mV in symmetric cells at 0.5 mA cm^{-2}. When coupled with a $LiFePO_4$ cathode, an improved rate capability is achieved as well.

1. Introduction

To keep up with growing demands for high energy density battery, Li metal is the most promising anode material owing to its high theoretical capacity (3860 mAh g^{-1}), the lowest redox potential (−3.04 V vs SHE) and light weight (0.53 g cm^{-3}) [1–4]. These properties make Li metal more competitive than conventional graphite anode material (370 mAh g^{-1}) of lithium-ion batteries. Nevertheless, the uneven top surface of Li metal may serve as charge accumulation spots leading to the infinite volume change, the irregular nucleation and dendrite growth of Li. The dendrites will fall out during repeating plating/stripping to form “dead Li”, causing low coulombic efficiency (CE) and sustained capacity fading [5–10]. Therefore, introducing uniform Li nucleation sites as well as depositing Li in a dense and reversible manner is crucial for the next-generation batteries based on Li metal anodes.

Up to now, various strategies have been proposed to overcome the formation of Li dendrites and the continuous breaking of solid electrolyte interface (SEI) on Li-anode surface. Substantial efforts have been made to enhance the chemical stability of the autogenetic SEI by introducing additives into electrolytes [11–13]. Other approaches such as the construction of artificial protective layer [14,15] or solid electrolyte [16–18] to enhance the interfacial mechanical strength have also been proposed. In spite of the effectively suppressed Li-dendrites, the large volume variation of Li metal under high current densities have not yet been well resolved. Alternatively, the 3D porous structure provides sufficient buffer space for internal stress caused by Li plating/stripping. Therefore, storing Li into 3D porous hosts with large specific surface area holds great promise to mitigate volume change and meanwhile reduces local current density. In recent studies, trials and tries on 3D hosts including copper foam [19,20] nickel foam [21,22] hollow carbon sphere [23] carbon nanofibers [24,25] graphene oxides [26–28] and polymer networks [29] have been done to store Li. Unfortunately, Cu, Ni and most carbon-based materials show poor wettability toward Li, and its uniform nucleation cannot to be achieved readily. Fortunately, some lithiophilic metals such as Ag [25,30], Au [31], Sn [32], Mg [33] and Zn [20] sheds brighter light to be applied as host materials. Besides, the metal oxide materials (ZnO [21], CuO [34], CoO [35], etc) have also shown the ability to improve the surface lithiophilicity. Therefore, developing host composites that combination of 3D structure with large specific surface area and high Li affinity is a plausible strategy. However, the usually applied process to prepare such composite materials is complicated which greatly impede their commercialization. A simple and efficient preparation method of an effective lithiophilic composite is still in urgent need.

* Corresponding author.
E-mail address: linawang@dhu.edu.cn (L. Wang).

https://doi.org/10.1016/j.coco.2021.100789
Received 24 April 2021; Received in revised form 8 May 2021; Accepted 8 May 2021
Available online 20 May 2021

In this work, we propose a flexible host of ZnO decorated carbon nanofibers (ZnO/CNFs) that prepared via electrospinning technique followed by a simple heat treatment for Li metal anode. The strong interaction between ZnO crystalline grains and CNFs is guaranteed by the atomic dispersion of zinc acetate in the precursor solution. The ZnO-enriched lithiophilic porous CNFs is effective for Li plating/stripping. First, the freestanding interconnected fibrous structure with enough mechanical strength can accommodate Li storage and buffer internal stress. Secondly, the high specific surface area of hierarchical porous CNFs can effectively decrease the local current density according to Sand's time low [36]. Thirdly, the electrical conductive carbon skeleton enables the fast electron transportation. More importantly, the uniformly distributed ZnO acting as continuous Li^+-modulating sites lead to the eventual suppression of Li dendrite growth. Therefore, the ZnO/CNFs@Li composite anode exhibits long-term stability for 1900 h with a low voltage hysteresis of 21.7 mV at 0.5 mA cm^{-2}. When paired with a $LiFePO_4$ (LFP) cathode, the reversible capacities can be preserved at 93.8 and 73.5 mAh g^{-1} at 5 C (1C = 170 mA g^{-1}) and 10 C, respectively.

2. Experimental section

2.1. Material synthesis

Zinc acetate ($Zn(CH_3COO)_2$, 98%, Sinopharm), polymethyl methacrylate (PMMA, Mw = 120,000, Sigma-Aldrich), polyacrylonitrile (PAN, Mw = 150,000, Sigma-Aldrich) and *N*,*N*-dimethylformamide (DMF, 99.5%, Shanghai Lingfeng Chemical) were used as received. ZnO/CNFs nanofibers were obtained by one-step electrospinning technique followed by heat-treatment. Typically, the solution of DMF (9.0 g) with dissolved PMMA (0.3333 g) and zinc acetate (1 g) was prepared firstly. Then, 0.6667 g of PAN was added into the solution and stirred for 12 h to obtain a clear solution. The solution was inhaled into an injector (5 mL) with the electrospinning voltage was 15 kV and the feeding rate was 0.5 μL min^{-1}. The distance between the receiving roller and needle was 20.0 cm. The dried fiber was firstly placed into a tube furnace at 280 °C for 2 h in air and then carbonized at 800 °C in N_2. As for CNFs, the synthesis process was the same as ZnO/CNFs except for the addition of zinc acetate.

2.2. Material characterizations

The morphological images were attained from a field-emission scanning electron microscope (SEM, 7500F, JEOL) and transmission electron microscope (TEM, JEM-2100F, JEOL) combined with Energy-dispersive X-ray spectroscopy (EDS). The X-ray diffraction (XRD, D/max-2500VB+/PC, Rigalcu) patterns were measured by a Cu-Kα radiation at a scan rate of 4° min^{-1}. A Quadrasorb adsorption instrument (Quantachrome Instruments) was used for nitrogen sorption/desorption measurements. The specific surface area was calculated according to the multipoint Brunauer-Emmett-Teller (BET) method. Raman spectra were detected from an inVia Reflex Raman Spectrometer (523 nm, inVia-Reflex, Renishaw). Thermogravimetry (TG) was conducted on a TG-DSC analyzer (NETZSCH TG 209 F1 Libra) with a heating rate of 10 °C min^{-1} in N_2 atmosphere.

2.3. Electrochemical measurements

The CR2025-type coin cells were assembled in an Ar-filled glove box (<0.1 ppm of H_2O and O_2, Mikrouna Universal) to investigate the electrochemical performance. The as-prepared ZnO/CNFs, CNFs and Cu foil were punched into disks with a diameter of 12.00 mm as the working electrode and Li foil as the counter electrode to evaluate the coulombic efficiency (CE) and Li deposition behavior. The electrolyte was 1, 3-dioxolane (DOL)/1, 2-dimethoxyethane (DME) (1/1, v/v) (Shanghai Song jing energy Co., LTD) containing1M lithium bis (trifluoromethanesulfonyl) imide (LiTFSI) and 0.2M lithium nitrate ($LiNO_3$). The amount of electrolyte in each cell is 60 μL. Polypropylene/polyethylene (PP/PE) microporous membrane (Celgard 2325) was used as the separator. The galvanostatic charge–discharge performance was tested on a LAND battery testing system (CT2001A) under room temperature of 25 °C. For symmetric cells, 10 mAh cm^{-2} of Li were predepositied onto working electrode, then the cells were disassembled in glove box and the electrodes were washed by DME (≥99%, Sigma-Aldrich). After that, the as obtained electrodes were re-assembled as ZnO/CNFs@Li||ZnO/CNFs@Li, CNFs@Li||CNFs@Li and Cu@Li||Cu@Li symmetrical cells. Electrochemical impedance spectra (EIS) were performed on CHI660E electrochemical workstation with an AC perturbation signal of 5.0 mV in the frequency range of 100 kHz–100 mHz (Shanghai Chenhua, China).

For full cell test, Cu@Li, CNFs@Li or ZnO/CNFs@Li composites with pre-depositied Li of 10 mAh cm^{-2} were used as the anode, respectively, and LFP was used as the cathode. In preparing the cathodes, black viscous slurry consisted of LFP (Shenzhen Dynanonic Co. LTD), carbon black (Acetylene, 99.9%, Alfa Aesar), and poly (vinylidene fluoride) (PVdF, HSV900) with a weight ratio of 90:5:5 was cast onto Al foil. The cathodes with a diameter of 12 mm were used to assemble CR2025 coin cells after dried under vacuum at 120 °C overnight. The LFP loading of the cathode is ca. 5 mg cm^{-2}. The cells were galvanostatically cycled at various current densities in the voltage of 2.0–4.0 V (vs Li^+/Li).

3. Results and discussion

3.1. Synthesis and characterization

The overall synthetic procedure involves a simple electrospinning procedure and subsequent thermal treatment (Fig. 1a). The electrospun precursor films were made from the solution of *N*,*N*-dimethylformamide (DMF) containing polyacrylonitrile (PAN), polymethyl methacrylate (PMMA) and zinc acetate ($(CH_3COO)_2Zn$). Whereby, PAN provides the desirable rheological properties as well as the carbon source, and PMMA acting as sacrifice additives to create porous structure in CNFs. Then, the as-spun films were thermally treated in N_2 flow at 800 °C for 2 h to obtain ZnO/CNFs composites. During the heating process of the precursor, the mass loss mainly occurs at 150–400 °C, which can be interpreted as the carbonization of PAN, the sublimation of PMMA and the formation of ZnO (Fig. 1b). Compared to the neat CNFs, the XRD pattern of ZnO/CNFs confirms the well crystallized phase of the in-situ generated ZnO (PDF# 36–1451, Fig. 1c) [21]. Raman spectra of both CNFs and ZnO/CNFs show characteristic peaks at 1352 and 1591 cm^{-1} (Fig. S1), corresponding to the disorder induced D-band and in-plane vibrational G-band, respectively [37]. The intensity ratio of D to G band (I_D/I_G) is 0.97 for CNFs and 1.08 for ZnO/CNFs. A higher I_D/I_G reflects a higher degree of disordered carbon.

The specific surface area is calculated based on the Brunauer-Emmet-Teller (BET) analysis (Fig. 1d). The nitrogen sorption/desorption isotherm of ZnO/CNFs exhibits a much higher surface area of 267.01 m^2 g^{-1}, compared to that of 19.26 m^2 g^{-1} for the CNFs. The pore width distribution suggests that micropores and mesopores smaller than 50 nm were generated inside the CNFs during heat treatment (Fig. 1e). Whereas, large volumes of additional macropores that mainly fell in the range of 55–200 nm were created in the ZnO/CNFs nanofibers, which should be resulted from the pyrolyzation of $(CH_3COO)_2Zn$ to release CO_2 etc. The scanning electron microscopy (SEM) images shield more light on the microstructure of ZnO/CNFs (Fig. 2a) and CNFs (Fig. 2b), both of which show an interconnected 3D fibrous network with a similar diameter ca. 300 nm of the single fiber (inset white box in Fig. 2a,b). Parallel internal channels can be clearly observed from the cross-sectional view of the single fiber (inset red box in Fig. 2a). Such parallel internal channels were resulted from the sublimation of PMMA [38], which can also be observed inside the CNFs (Fig. S2). As a contrast, the mostly common Cu foil reveals a moss-like surface (Fig. 2c).

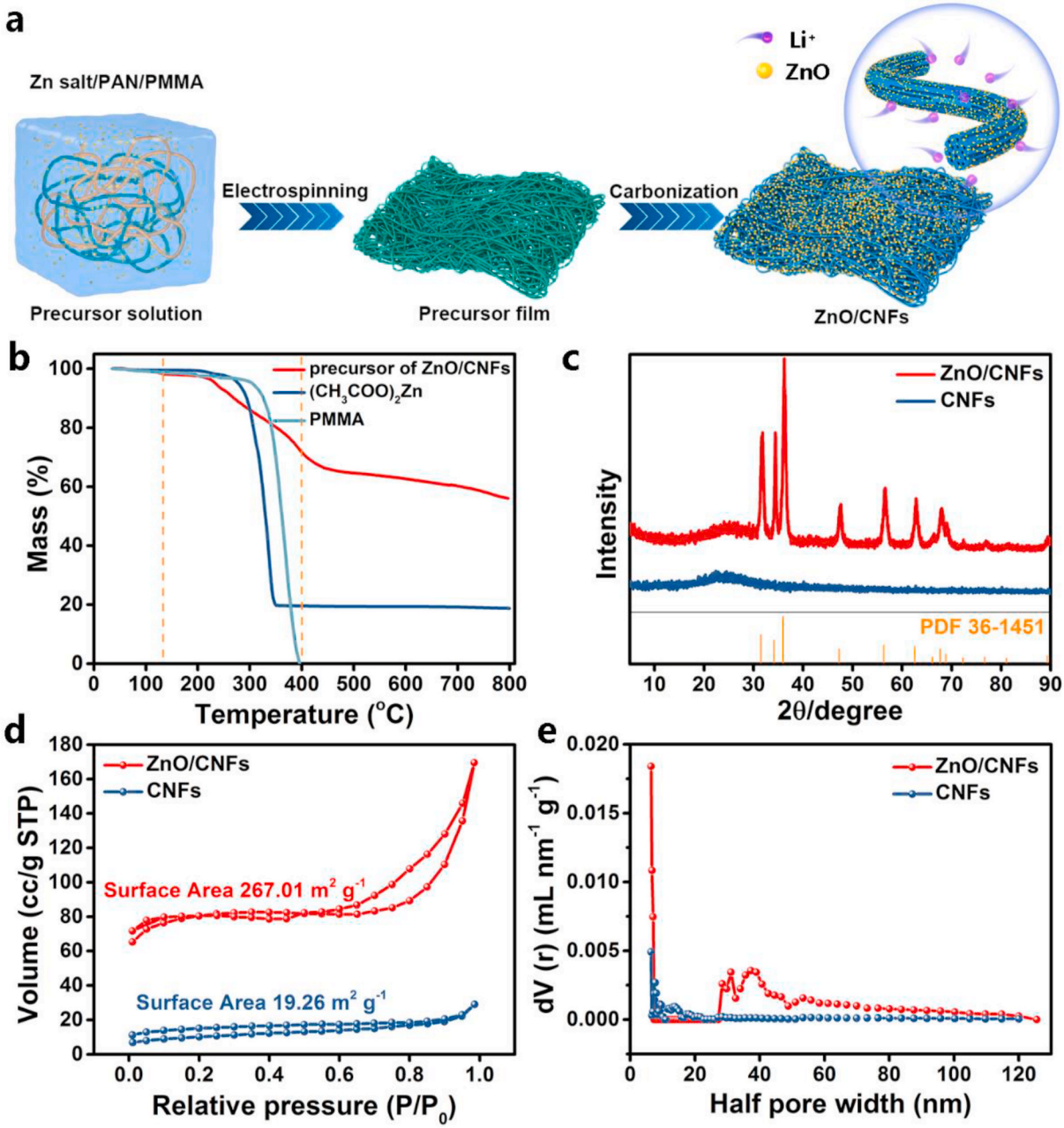

Fig. 1. (a) Schematic illustration of the synthesis process of ZnO/CNFs. (b) TGA of PMMA, $(CH_3COO)_2Zn$ and precursor of ZnO/CNFs. (c) XRD patterns, (d) nitrogen sorption/desorption isotherms and (e) pore-size distributions of the CNFs and ZnO/CNFs.

Transmission electron microscopy (TEM) images show the surface of ZnO/CNFs is smooth (Fig. 2d). The uniform distribution of the Zn, O, C and N elements was identified by energy-dispersive X-ray spectroscopy (EDS) element mapping images (Fig. 2e).

3.2. Lithium plating behavior of ZnO/CNFs

To investigate the Li plating behavior, 10 mAh cm^{-2} of Li was electrodeposited onto ZnO/CNFs, CNFs and Cu at 0.5 mA cm^{-2} to obtain the ZnO/CNFs@Li, CNFs@Li and Cu@Li composite electrodes, respectively. For ZnO/CNFs@Li, a thin layer of Li was uniformly covered over through the fibers (Fig. 2f). However, bulk Li can be seen on the top surface of CNF@Li, suggesting its weak interaction with Li (Fig. 2g). As for planar Cu@Li, the massive Li nucleus can be clearly seen from SEM images (Fig. 2h). The digital images of as-disassembled cells show there is no visible silvery Li layer on the top surface of ZnO/CNFs@Li electrode (Fig. S3a). However, the silvery Li layer resulted from the inhomogeneous Li plating can be observed on the CNFs@Li (Fig. S3b) and Cu@Li foil (Fig. S3c). The cross-sectional SEM images more clearly shows that the Li uniformly covers over the single fiber rather than gathers on top of ZnO/CNFs electrode (Fig. 2i). Whereas it can be more clearly observed that the Li mainly plated on the top of CNF rather than filled inside the 3D scaffold (Fig. 2j). These massive Li exhibits a distinct boundary with the Cu foil, indicating the weak mechanical stacking (Fig. 2k).

For further clarification, SEM was performed to probe the Li plating behavior at other current densities. For comparision, 10 mAh cm^{-2} of lithium were deposited at the current densities of 0.1, 0.75 and 1 mA cm^{-2}, respectively. With the current density increasing, the amounts of Li nucleus gradually increase on Cu foil, result in the final morphology of Li transfers from block to strip (Fig. 3a). The uncontrolled bulk Li plating is observed on the CNFs at higher current densities (Fig. 3b). For ZnO/

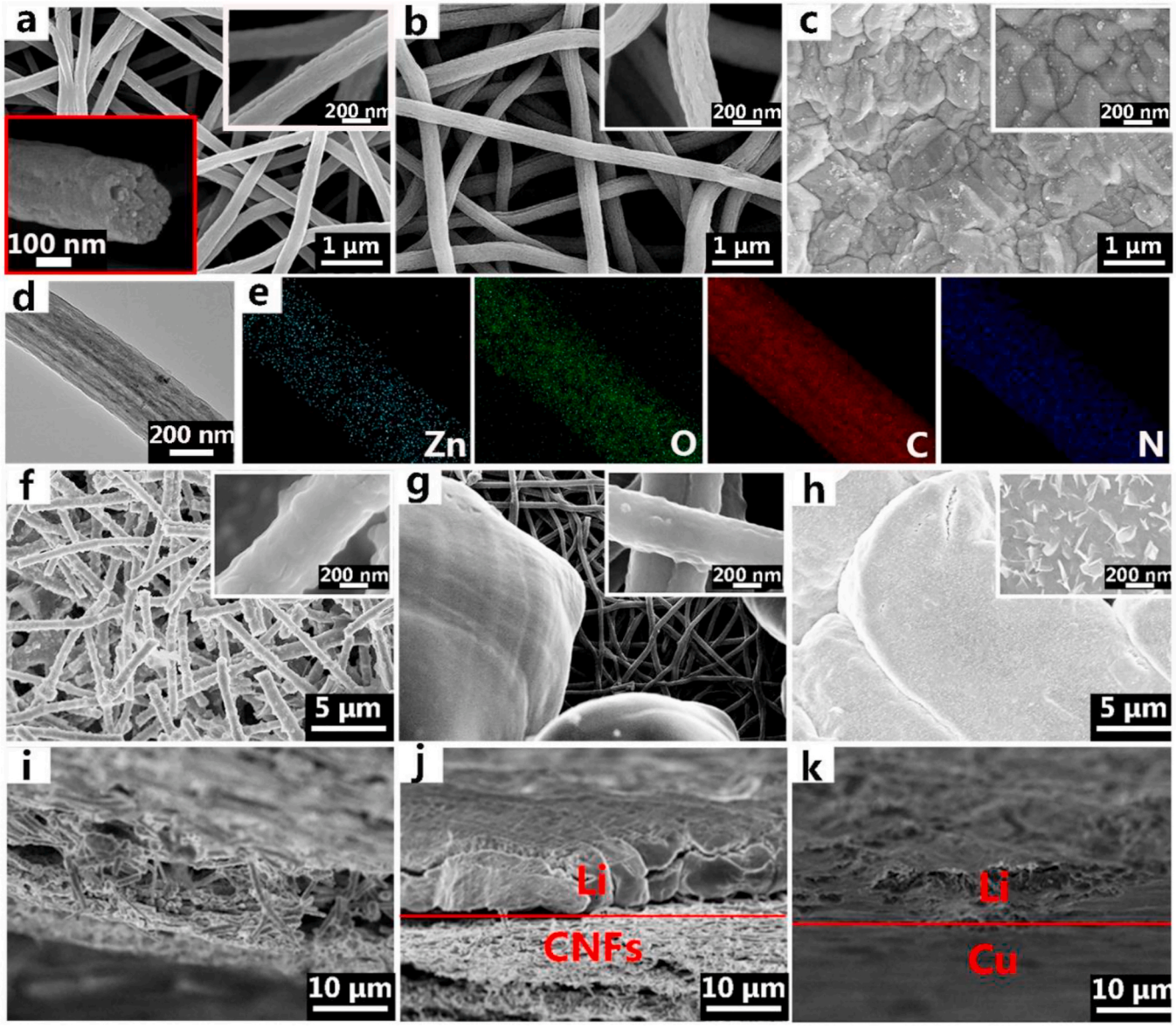

Fig. 2. SEM images of (a) ZnO/CNFs, (b) CNFs and (c) Cu foil. The inset white boxes are images with high magnifications. The inset red box of (a) is the cross section image of single nanofiber of ZnO/CNFs. (d) TEM image of ZnO/CNFs and (e) the corresponding elemental mapping of Zn, O, C and N. Top-view SEM images of (f) ZnO/CNFs@Li, (g) CNFs@Li, (h) Cu@Li after plating 10 mAh cm^{-2} of Li at 0.5 mA cm^{-2}. The corresponding cross-sectional view of (i) ZnO/CNFs@Li, (j) CNFs@Li, (k) Cu@Li. (For interpretation of the references to colour in this figure legend, the reader is referred to the Web version of this article.)

CNFs electrode, the Li uniformly plating over the fiber surface without bulk appears irrespective of the current densities (Fig. 3c), indicating the ZnO decorated CNFs is a favorable construction to regulate the Li distribution as well as to buffer the volume change.

3.3. Electrochemical characteristics of ZnO/CNFs

The nucleation overpotential is an intuitive parameter to evaluate the lithiophilic property of host. Generally, a sharp voltage drop related to the nucleation process of Li appears during the initial plating process (Fig. 4a). After that, the voltage shows slight rise and finally reaches to a stable plateau, which represents the mass-transfer-controlled overpotential. The voltage difference between sharp tip and stable platform is defined as the nucleation overpotential. At 0.5 mA cm^{-2}, the Cu foil exhibits a high nucleation overpotential of 34 mV (Inset in Fig. 4a). The high specific surface area of 3D skeleton can significantly reduce the local current densities thus leading to much smaller nucleation overpotential of ZnO/CNFs and CNFs. In contrast, the ZnO/CNFs exhibits a smaller nucleation overpotential of 7 mV than that of 12 mV for CNFs, suggesting the enhanced Li affinity of ZnO/CNFs due to the positive effect of well distributed ZnO crystalline grains. Before Li plating process at ca. 0 V, three plateaus appear in the voltage profiles of ZnO/CNFs during the initial discharge process (Fig. S4). The first and second plateaus at ca. 1.7 and 0.9 V (vs. Li/Li^+) are caused by the parasitic reaction between Li^+ and CN bonds and the Li adsorption into the porous structure of nanofibers, respectively, and both of two reactions are poorly reversible [38,39]. The third plateau at ca. 0.5 V refers to the electrochemical reaction between ZnO and Li ($Li + ZnO \rightarrow LiZn + Li_2O$). Upon striping, the Li is extracted from LiZn to form Zn, with Li_2O remaining as an irreversible inactive phase ($LiZn + Li_2O \rightarrow Li + Zn + Li_2O$) [40,41]. In the following cycles, the electrochemical reaction happens reversibly between Li and Zn ($Li + Zn \leftrightarrow LiZn$). Therefore, the Zn would act as the lithiophilic sites for repeating and smooth Li plating/stripping.

The nucleation overpotential at various current densities were also investigated (Fig. 4b). The nucleation overpotential of Cu increases from

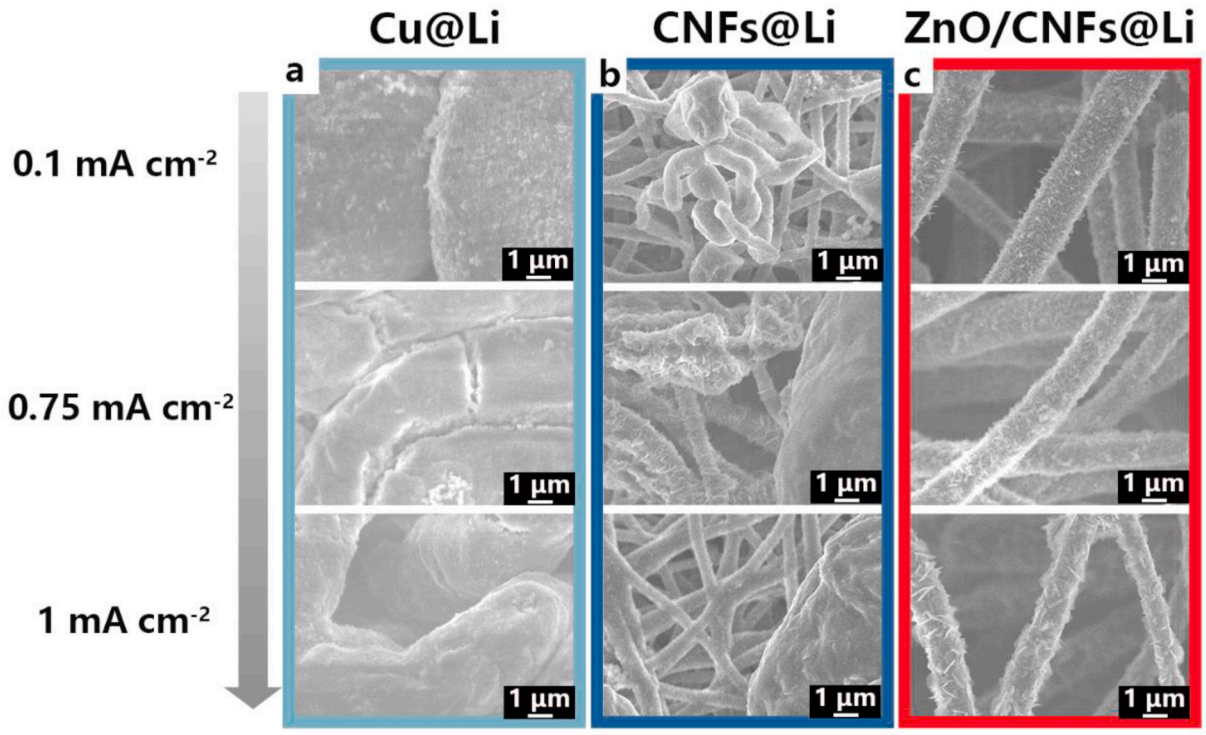

Fig. 3. SEM images of (a) Cu@Li, (b) CNF@Li and (c) ZnO/CNFs@Li after plating 10 mAh cm^{-2} of Li at various current densities from 0.1 to 1 mA cm^{-2}.

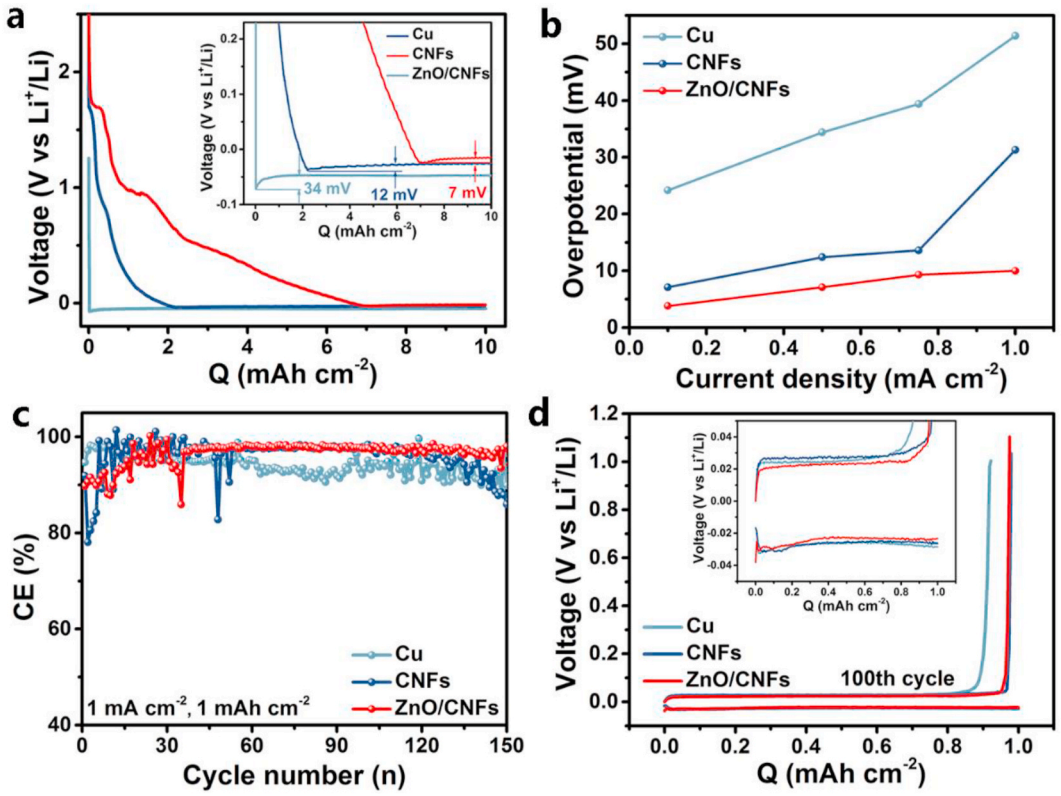

Fig. 4. The Li nucleation overpotential of ZnO/CNFs, CNFs, and Cu electrodes at (a) 0.5 mA cm^{-2} and (b) various current densities. (c) The Coulombic efficiency of ZnO/CNFs, CNFs and Cu at 1 mA cm^{-2} with a fixed capacity of 1 mAh cm^{-2}, and (d) the corresponding voltage–capacity profiles at 100th cycle.

24.2 to 51.4 mV with increasing of current density from 0.1 to 1 mA cm^{-2}, and which is 7.2–31.3 mV for CNFs. Impressively, the nucleation overpotential for ZnO/CNFs is only increased from 3.8 to 10 mV, suggesting the Li nucleation can be regulated at high densities. To evaluate the coulombic efficiency (CE), half cells were assembled by pairing Cu, CNF and ZnO/CNFs electrodes with Li foil. The cells were

discharged at 1 mA cm^{-2} with a capacity of 1 mAh cm^{-2} and then charged to 1.0 V (Fig. 4c). After an initial activation process, the CE of ZnO/CNFs increases from 89.8% to 98% and maintains over 150 cycles. The CE of Cu foil and CNF drops below 89% and 86%. The obvious irreversible capacity of Cu foil can be clearly seen from the discharge–charge profiles (Fig. 4d). Among which, the ZnO/CNFs displays the highest CE as well as the lowest overpotential (Inset in Fig. 4d).

The cyclic performance of symmetrical cells of Cu@Li, CNF@Li and ZnO/CNFs@Li electrodes were measured with a fixed capacity of 1 mAh cm^{-2} at current density of 0.5, 1, 2 mA cm^{-2}, respectively. The representative plating–stripping profiles are shown in Fig. S5. The ZnO/CNFs demonstrates a long cycle life over 1900 h and a small voltage hysteresis ca. 21.7 mV at 0.5 mA cm^{-2} (Fig. 5a). However, the CNF@Li and Cu@Li electrodes only sustain 550 h and 200 h with an abrupt resistance increase. At 1 mA cm^{-2}, a relatively stable cycling over 1300 h with a hysteresis of 50 mV can be achieved for ZnO/CNFs@Li (Fig. 5b). CNF@Li suffers from a gradually increased polarization and Cu@Li deteriorates rapidly after only 35 cycles (70 h). The advantage of ZnO/CNFs@Li can be further demonstrated at 2 mA cm^{-2} (Fig. 5c). The huge continuous increase in voltage hysteresis of Cu@Li suggests an internal polarization caused by the "dead Li". The CNF@Li sustains for 110 cycles (110 h) with a voltage hysteresis of 69.8 mV. And the ZnO/CNFs@Li shows much better cyclic stability up to 300 cycles (300 h). The rate performance of these symmetrical cells are measured as well with a fixed capacity of 1 mAh cm^{-2} (Fig. 5d). A small voltage hysteresis of 81.8, 59, 40.4 and 24.2 mV can be recovered from 3 to 0.5 mA cm^{-2}, indicating that the ZnO/CNFs@Li can effectively regulate the Li deposition behaviors. The electrochemical impedance spectrum (EIS) was employed to measure the interfacial charge transfer resistance (R_{ct}) before and after symmetrical cell test (Fig. S6). The fresh ZnO/CNFs@Li exhibits a lower R_{ct} of 30.6 Ω than CNF@Li (39.2 Ω) and Cu@Li (45.9 Ω). After 10 cycles at 0.5 mA cm^{-2}, the ZnO/CNFs@Li (4.5 Ω) electrode also delivers the lowest resistance than CNF@Li (5.4 Ω) and Cu@Li (10.6 Ω), implying a faster electrochemical reaction kinetics.

To further demonstrate the feasibility of as-prepared ZnO/CNFs for practical applications, the Cu@Li, CNF@Li and ZnO/CNFs@Li anodes were coupled with a LFP cathode, respectively, to be tested from 0.2 to 10 C in the voltage range of 2.0–4.0 V (Fig. 5e,f). Compared to Cu@Li||LFP and CNF@Li||LFP, ZnO/CNFs@Li||LFP delivers the highest discharge capacity of 157.7, 149.1, 138.8, 121.3, 94.1 and 73.5 mAh g^{-1} along with a stable CE of 99.8% at 0.2, 0.5, 1, 2, 5 and 10 C, respectively. On going from 10 to 0.2 C, a high capacity of 155.6 mAh g^{-1} can be recovered, indicating that ZnO/CNFs host indeed is beneficial for uniform and dendrite-free Li deposition and regulate the volume change of Li metal.

4. Conclusions

In summary, this work demonstrates the enhanced lithiophilic property of porous carbon nanofibers with uniformly distributed ZnO

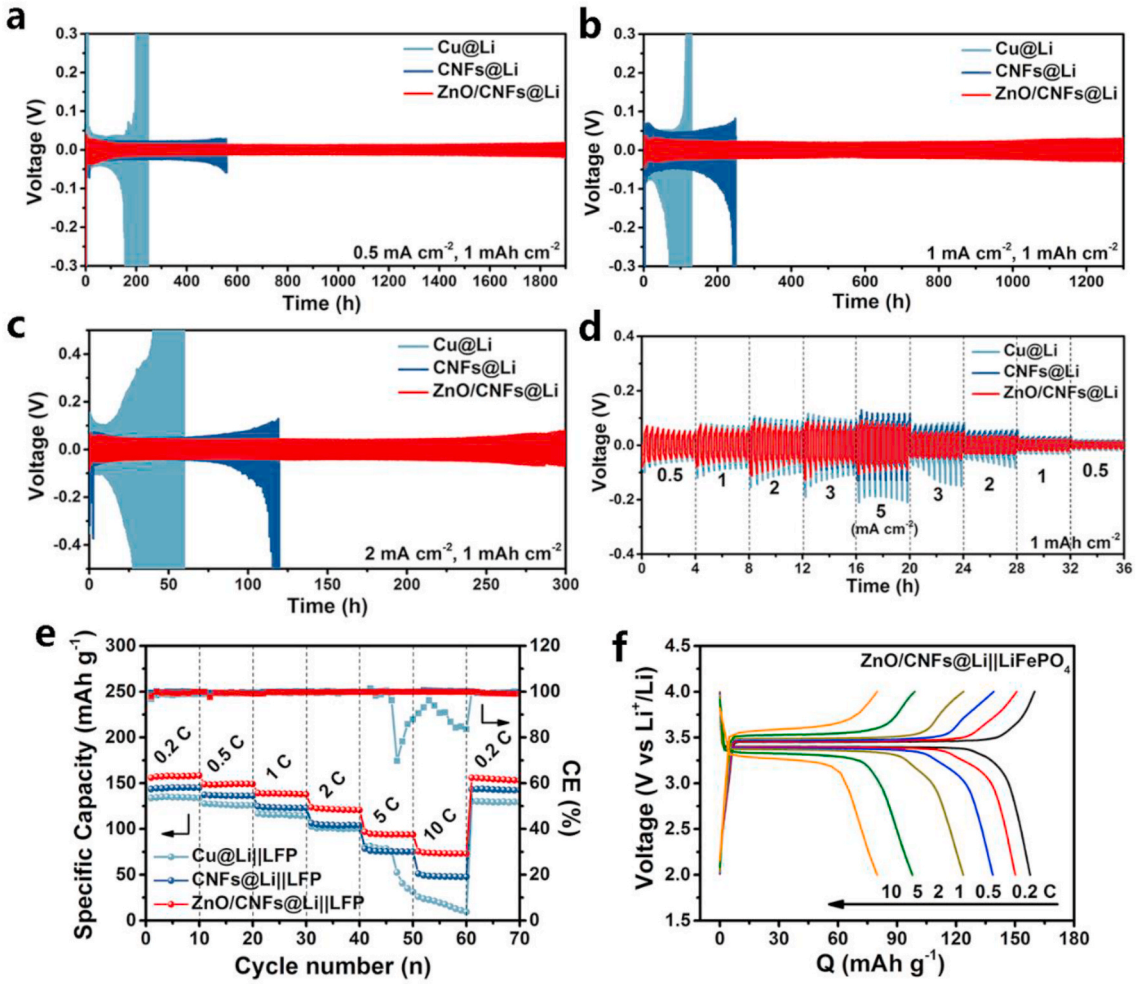

Fig. 5. Galvanostatic cycling performance of symmetric cells with ZnO/CNFs@Li, CNFs@Li and Cu@Li electrodes at (a) 0.5, (b) 1, and (c) 2 mA cm^{-2}. (d) Rate capability of the three symmetrical cells. The platting/stripping capacity was limited to 1 mAh cm^{-2}. (e) Rate performance of ZnO/CNFs@Li||LFP, CNFs@Li||LFP and Cu@Li||LFP full cells. (b) Voltage–capacity profiles at various current rates from 0.2 to 10C of ZnO/CNFs@Li||LFP.

crystalline grains. The flexible and freestanding ZnO/CNFs network was prepared through electrospinning method followed by simple heat treatment. Due to the decoration of the lithiophilic ZnO, the lithiophobic nature of CNFs is transformed into lithiophilic, which largely reducing the nucleation barrier of Li. Moreover, the 3D porous structure effectively reduces the local current density especially at high rates. As a result, the ZnO/CNFs enables a dendrite free Li plating behavior. A long-term cycling stability over 1900 h at 0.5 mA cm^{-2} can be achieved for the symmetric cells with ZnO/CNFs@Li composite electrode. By integrating of ZnO/CNFs@Li with a LFP cathode, decent rate capability can be acquired. The strategy is promising for the next-generation Li metal batteries in view of the scalable and simple fabrication process for 3D host.

CRediT authorship contribution statement

Chengcheng Zhao: Investigation, Methodology, Writing – original draft, Writing – review & editing, Software, Visualization. **Xiao Yao:** Data curation, Visualization, Formal analysis. **Hao Yang:** Investigation, Formal analysis, Methodology, Conceptualization. **Xiaoxia Jiao:** Formal analysis, Investigation. **Lina Wang:** Methodology, Writing – original draft, Writing – review & editing, Visualization, Supervision, Funding acquisition.

Declaration of competing interest

The authors declare that they have no known competing financial interests or personal relationships that could have appeared to influence the work reported in this paper.

Acknowledgements

The authors acknowledge funding support from the National Natural Science Foundation of China (No. 21603030), the Natural Science Foundation of Shanghai (No. 17ZR1446400), and the Shanghai Scientific and Technological Innovation Project (No. 18JC1410600).

Appendix A. Supplementary data

Supplementary data to this article can be found online at https://doi.org/10.1016/j.coco.2021.100789.

References

[1] J. Tarascon, M. Armand, Issues and challenges facing rechargeable lithium batteries, Nature 414 (2001) 359–367.
[2] P. Bruce, S. Freunberger, L. Hardwick, J. Tarascon, Li-O_2 and Li–S batteries with high energy storage, Nat. Mater. 11 (2011) 19–29.
[3] C. Yang, Y. Yin, S. Zhang, N. Li, Y. Guo, Accommodating lithium into 3D current collectors with a submicron skeleton towards long-life lithium metal anodes, Nat. Commun. 6 (2015) 8058–8067.
[4] W. Xu, J. Wang, F. Ding, X. Chen, E. Nasybutin, Y. Zhang, J. Zhang, Lithium metal anodes for rechargeable batteries, Energy Environ. Sci. 7 (2014) 513–537.
[5] Y. Zhao, L. Goncharova, Q. Zhang, P. Kaghazchi, Q. Sun, A. Lushington, B. Wang, R. Li, X. Sun, Inorganic–Organic coating via molecular layer deposition enables long life sodium metal anode, Nano Lett. 17 (2017) 5653–5659.
[6] X. Cheng, R. Zhang, C. Zhao, Q. Zhang, Toward safe lithium metal anode in rechargeable batteries: a review, Chem. Rev. 117 (2017) 10403–10473.
[7] P. Bai, J. Li, F. Brushett, M. Bazant, Transition of lithium growth mechanisms in liquid electrolytes, Energy Environ. Sci. 9 (2016) 3221–3229.
[8] P. Hundekar, S. Basu, J. Pan, S. Bartolucci, S. Narayanan, Z. Yang, N. Koratkar, Exploiting self-heat in a lithium metal battery for dendrite healing, Energy Storage Mater. 20 (2019) 291–298.
[9] C. Yang, K. Fu, Y. Zhang, E. Hitz, L. Hu, Protected lithium-metal anodes in batteries from liquid to solid, Adv. Mater. 29 (2017) 1701169.
[10] Y. Zhang, Y. Shi, X. Hu, W. Wang, R. Wen, S. Xin, Y. Guo, A 3D lithium/carbon fiber anode with sustained electrolyte contact for solid-state batteries, Adv. Energy Mater. 10 (2019) 1903325.
[11] A. Thenuwara, P. Shetty, N. Kondekar, S. Sandoval, K. Cavallaro, R. May, C. Yang, L. Marbella, Y. Qi, M. McDowell, Efficient low-temperature cycling of lithium metal anodes by tailoring the solid-electrolyte interphase, ACS Energy Lett. 5 (2020) 2411–2420.
[12] Z. Lu, W. Li, Y. Long, J. Liang, Q. Liang, S. Wu, Y. Tao, Z. Weng, W. Lv, Q. Yang, Constructing a high-strength solid electrolyte layer by in vivo alloying with aluminum for an ultrahigh-rate lithium metal anode, Adv. Funct. Mater. 30 (2019) 1907343.
[13] S. Lang, Z. Shen, X. Hu, Y. Shi, Y. Guo, F. Jia, F. Wang, R. Wen, L. Wan, Tunable structure and dynamics of solid electrolyte interphase at lithium metal anode, Nano Energy 75 (2020) 104967.
[14] Z. Hu, F. Liu, J. Gao, W. Zhou, H. Huo, J. Zhou, L. Li, Dendrite-free lithium plating induced by in situ transferring protection layer from separator, Adv. Funct. Mater. 30 (2019) 1907020.
[15] Y. Liu, D. Lin, P. Yuen, K. Liu, J. Xie, R. Dauskardt, Y. Cui, An artificial solid electrolyte interphase with high Li–ion conductivity, mechanical strength, and flexibility for stable lithium metal anodes, Adv. Mater. 29 (2017) 1605531.
[16] X. Li, J. Liang, J. Luo, M. Banis, C. Wang, W. Li, S. Deng, C. Yu, F. Zhao, Y. Hu, T. Sham, L. Zhang, S. Zhao, S. Lu, H. Huang, R. Li, K. Adaira, X. Sun, Air-stable Li_3InCl_6 electrolyte with high voltage compatibility for all-solid-state batteries, Energy Environ. Sci. 12 (2019) 2665–2671.
[17] W. Ping, C. Yang, Y. Bao, C. Wang, H. Xie, E. Hitz, J. Cheng, T. Li, L. Hu, A silicon anode for Garnet-based all-solid-state batteries: interfaces and nanomechanics, Energy Storage Mater. 21 (2019) 246–252.
[18] Q. Zhang, D. Cao, Y. Ma, A. Natan, P. Aurora, H. Zhu, Sulfide-based solid-state electrolytes: synthesis, stability, and potential for all-solid-state batteries, Adv. Mater. 31 (2019) 1901131.
[19] J. Chen, J. Zhao, L. Lei, P. Li, J. Chen, Y. Zhang, Y. Wang, Y. Ma, D. Wang, Dynamic intelligent Cu current collectors for ultrastable lithium metal anodes, Nano Lett. 20 (2020) 3403–3410.
[20] S. Kim, Y. Kim, C. Nguyen, T. Jang, H. Lee, H. Byon, Promoting lithium electrodeposition towards the bottom of 3D copper meshes in lithium-based batteries, J. Power Sources 472 (2020) 228495.
[21] C. Sun, Y. Li, J. Jin, J. Yang, Z. Wen, ZnO nanoarrays modified nickel foam as a lithiophilic skeleton to regulate lithium deposition for lithium-metal batteries, J. Mater. Chem. 7 (2019) 7752–7759.
[22] Z. Lu, Q. Liang, B. Wang, Y. Tao, Y. Zhao, W. Lv, D. Liu, C. Zhang, Z. Weng, J. Liang, H. Li, Q. Yang, Graphitic carbon nitride induced micro-electric field for dendrite-free lithium metal anodes, Adv. Energy Mater. 9 (2019) 1803186.
[23] K. Yan, Z. Lu, H. Lee, F. Xiong, P. Hsu, Y. Li, J. Zhao, S. Chu, Y. Cui, Selective deposition and stable encapsulation of lithium through heterogeneous seeded growth, Nat. Energy 1 (2016) 16010.
[24] K. Lin, X. Qin, M. Liu, X. Xu, G. Liang, J. Wu, F. Kang, G. Chen, B. Li, Ultrafine titanium nitride sheath decorated carbon nanofiber network enabling stable lithium metal anodes, Adv. Funct. Mater. 29 (2019) 1903229.
[25] C. Yang, Y. Yao, S. He, H. Xie, E. Hitz, L. Hu, Ultrafine silver nanoparticles for seeded lithium deposition toward stable lithium metal anode, Adv. Mater. 29 (2017) 1702714.
[26] Y. Gong, J. Heo, H. Lee, H. Kim, J. Cho, S. Pyo, H. Yun, H. Kim, S. Park, J. Yoo, Y. Kim, Li metal anodes: nonwoven rGO fiber-aramid separator for high-speed charging and discharging of Li metal anode, Adv. Energy. Mater. 10 (2020) 2070119.
[27] R. Zhang, N. Wang, C. Shi, E. Liu, C. He, N. Zhao, Spatially uniform Li deposition realized by 3D continuous duct-like graphene host for high energy density Li metal anode, Carbon 161 (2020) 198–205.
[28] R. Zhang, X. Chen, X. Cheng, X. Zhang, C. Yan, Q. Zhang, Lithiophilic sites in doped graphene guide uniform lithium nucleation for dendrite-free lithium metal anodes, Angew. Chem. Int. Ed. 56 (2017) 7764–7768.
[29] M. Zhang, R. Lu, H. Yuan, K. Amin, L. Mao, W. Yan, Z. Wei, Nanowire array-coated flexible substrate to accommodate lithium plating for stable lithium-metal anodes and flexible lithium-organic batteries, ACS Appl. Mater. Interfaces 11 (2019) 20873–20880.
[30] Y. Yang, M. Zhao, H. Geng, Y. Zhang, Y. Fang, C. Li, J. Zhao, Three-dimensional graphene/Ag aerogel for durable and stable Li metal anodes in carbonate-based electrolytes, Chem. Eur. J. 25 (2019) 5036–5042.
[31] J. Chen, J. Xiang, X. Chen, L. Yuan, Z. Li, Y. Huang, Li_2S-based anode-free full batteries with modified Cu current collector, Energy Storage Mater. 30 (2020) 179–186.
[32] H. Qiu, T. Tang, M. Asif, W. Li, T. Zhang, Y. Hou, Stable lithium metal anode enabled by lithium metal partial alloying, Nano Energy 65 (2019) 103989.
[33] L. Kong, L. Wang, Z. Ni, S. Liu, G. Li, X. Gao, Lithium-magnesium alloy as a stable anode for lithium-sulfur battery, Adv. Funct. Mater. 29 (2019) 1808756.
[34] K. Huang, Z. Li, Q. Xu, H. Liu, H. Li, Y. Wang, Lithiophilic CuO nanoflowers on Ti-mesh inducing lithium lateral plating enabling stable lithium-metal anodes with ultrahigh rates and ultralong cycle life, Adv. Energy Mater. 9 (2019) 1900853.
[35] X. Yue, W. Wang, Q. Wang, J. Meng, Z. Zhang, X. Wu, X. Yang, Y. Zhou, CoO nanofiber decorated nickel foams as lithium dendrite suppressing host skeletons for high energy lithium metal batteries, Energy Storage Mater. 14 (2018) 335–344.
[36] C. Brissot, M. Rosso, J. Chazalviel, P. Baudry, S. Lascaud, In situ study of dendritic growth in lithium/PEO-salt/lithium cells, Electrochim. Acta 43 (1998) 1569–1574.
[37] H. Yang, C. Fu, Y. Sun, L. Wang, T. Liu, Fe-doped $LiMnPO_4$@C nanofibers with high Li-ion diffusion coefficient, Carbon 158 (2020) 102–109.
[38] C. Zhao, S. Xiong, H. Li, Z. Li, C. Qi, H. Yang, L. Wang, Y. Zhao, T. Liu, A dendrite-free composite Li metal anode enabled by lithiophilic Co, N codoped porous carbon nanofibers, J. Power Sources 481 (2021) 229188.
[39] X. Wang, Y. Qian, L. Wang, H. Yang, H. Li, Y. Zhao, T. Liu, Sulfurized polyacrylonitrile cathodes with high compatibility in both ether and carbonate

electrolytes for ultrastable lithium-sulfur batteries, Adv. Funct. Mater. 29 (2019) 1902929.

[40] M. Park, G. Sung, N. Sung, J. Kim, C. Park, Partially reversible Li_2O formation in ZnO: a critical finding supporting realization of highly reversible metal oxide electrodes, J. Power Sources 328 (2016) 607–614.

[41] X. Shen, D. Mu, S. Chen, B. Wu, F. Wu, Enhanced electrochemical performance of ZnO-Loaded/Porous carbon composite as anode materials for lithium ion batteries, ACS Appl. Mater. Interfaces 5 (2013) 3118–3125.